Quantitative Analysis of Nonequilibrium Phonon Transport Near a Nanoscale Hotspot

Jiaxuan Xu,[1] Yue Hu,[1] and Hua Bao[1,2,*]

[1] *University of Michigan-Shanghai Jiao Tong University Joint Institute, Shanghai Jiao Tong University, Shanghai 200240, People's Republic of China*

[2] *Global Institute of Future Technology, Shanghai Jiao Tong University, Shanghai 200240, People's Republic of China*

(Received 13 September 2022; revised 30 October 2022; accepted 2 December 2022; published 4 January 2023)

Understanding thermal transport by phonons near nanoscale hotspots is critical for many engineering applications, especially for nanoscale thermal measurements and nanoelectronics. Previous studies usually adopted the gray phonon Boltzmann transport equation to consider ballistic phonon transport or the multitemperature model to consider selective phonon excitation. However, nonequilibrium phonon transport near a nanoscale hotspot cannot be fully captured by either method. In this work, we employ the more rigorous nongray phonon Boltzmann transport equation to investigate phonon transport near nanoscale hotspots. We first consider hotspots in a one-dimensional system with two phonon modes to extract the underlying physics. Thermal transport is found to be less efficient near these hotspots, leading to significantly smaller effective thermal conductivity. The mechanism behind this is that different phonon modes have different temperatures and are therefore not in equilibrium. Nonequilibrium is caused by both the selective electron-phonon interaction and ballistic phonon transport. For relatively large hotspots, nonequilibrium is primarily contributed to by the selective excitation effect. When the hotspot size further reduces, the contribution from ballistic phonon transport becomes increasingly more important. Furthermore, we quantitatively study the thermal transport of laser-heated hotspots in Raman experiments and Joule heating in fin field-effect transistors (FETs) using the nongray phonon Boltzmann transport equation. We find that the measured thermal conductivity of single-layer graphene can be significantly underestimated if the nonequilibrium effect is ignored. Additionally, the peak temperature rise in a silicon fin FET is much larger than that calculated by the heat-diffusion equation.

DOI: 10.1103/PhysRevApplied.19.014007

I. INTRODUCTION

Nanoscale hotspots exist widely in many engineering applications, such as nanoscale optical pump-probe thermal measurements [1–3], electronics [4,5], optoelectronics [6], and quantum nanodevices [7]. Understanding the mechanism of thermal transport by phonons near nanoscale hotspots is vital to predict and improve the performance of these applications [8]. As many materials have phonons with mean free paths (MFPs) comparable to or even larger than the scale of nanoscale hotspots, thermal transport near these hotspots reaches the ballistic regime and no longer follows the Fourier-law-based heat-diffusion equation [9–11]. On the other hand, nanoscale hotspots are generally induced by optical or electrical excitation, in which the phonons are excited through the electron-phonon scattering process [12–15]. As the electrons can preferentially interact with some phonon modes, phonons in the hotspots are generally not excited equally, i.e., some phonon modes gain more energy than others, leading to selective phonon excitation [16,17]. Investigating these two common effects is significant for understanding the phonon-transport mechanism near nanoscale hotspots.

There have been extensive theoretical and experimental efforts to investigate phonon transport near nanoscale hotspots. It is found that the effective thermal conductivity decreases with shrinking size for a single nanoscale hotspot [18–20], which leads to higher temperature rises than the bulk Fourier prediction [21–23]. It is also shown that, when multiple nanoscale hotspots are tightly distributed to each other, the effective thermal conductivity anomalously recovers the bulk value [24–27]. In these works, the hotspots are usually regarded as an equilibrium heat source and the deviation in thermal conductivity is attributed to ballistic phonon transport [28–32]. On the other hand, there are also reports in the literature on phonon-temperature nonequilibrium induced by selective phonon excitation near nanoscale hotspots, where the local

*hua.bao@sjtu.edu.cn

thermal equilibrium assumption breaks down [17,33–36]. We refer to this local thermal nonequilibrium as phonon (temperature) nonequilibrium in subsequent sections. Vallabhaneni *et al.* [17] developed a multitemperature model based on diffusive transport theory to study laser-heated graphene, where the nonequilibrium temperatures of different phonon branches in suspended graphene were predicted. Such phonon-temperature nonequilibrium was later experimentally confirmed by Zobeiri *et al.* [36] and Dolleman *et al.* [34]. They found temperature nonequilibrium between optical and acoustic phonons and between in-plane and out-of-plane acoustic phonons near nanoscale hotspots in graphene using Raman spectroscopy and optomechanical techniques. In these works, although the branch-level phonon-temperature nonequilibrium is investigated, ballistic phonon transport is neglected. Despite these studies, it is necessary to consider selective phonon excitation and ballistic phonon transport in a unified quantitative framework to further understand thermal transport near a nanoscale hotspot.

Here, we employ the phonon Boltzmann transport equation (BTE) to study nonequilibrium phonon transport near a nanoscale hotspot. We first start with the theoretical framework of the phonon BTE and illustrate different origins that induce phonon nonequilibrium, including both selective phonon excitation and ballistic phonon transport. Taking nanoscale hotspots in one-dimensional (1D) systems as prototypes, we compare four different approaches to model phonon transport near hotspots to characterize the effects of both selective phonon excitation and ballistic phonon transport on phonon nonequilibrium and the effective thermal conductivity. Based on these understandings, we further quantitatively investigate nonequilibrium phonon transport near nanoscale hotspots in two practical applications, i.e., Raman laser heating a spot on suspended single-layer graphene and Joule heating a spot in a silicon bulk fin field-effect transistor (FET).

II. THEORETICAL ANALYSIS

A. Origins of phonon nonequilibrium

Near a nanoscale hotspot, the governing equation for thermal transport is the phonon BTE [37]:

$$\frac{\partial f}{\partial t}+\mathbf{v}\cdot\nabla f=\left(\frac{\partial f}{\partial t}\right)_s. \tag{1}$$

Here, $f=f(\mathbf{r},\hat{\mathbf{s}},\omega,p)$ is the phonon distribution function, which represents the fraction of phonons at position $\mathbf{r}$ in direction $\hat{\mathbf{s}}$ with frequency ω and polarization p [37]. $\mathbf{v}$ denotes the phonon group velocity. The phonon BTE describes the evolution of the phonon distribution function, where $\mathbf{v}\cdot\nabla f$ is the phonon-transport term; $(\partial f/\partial t)_s$ is the scattering term, which is dominated by phonon-phonon scattering and electron-phonon scattering for bulk and intrinsic materials [37–39]. The phonon BTE covers the entire ballistic-to-diffusive phonon-transport regime and inherently includes all effects that induce phonon nonequilibrium [40–42].

To understand nonequilibrium phonon transport near a nanoscale hotspot, we further assume that (1) the system is time invariant (steady state); (2) the electron-phonon scattering term can be reduced to a mode-dependent heat-generation term [43]; and (3) the phonon-phonon scattering term can be described by the relaxation-time approximation, which represents the energy exchange between different phonons due to phonon-phonon scattering processes [9]. By multiplying the phonon distribution function with the phonon energy, $\hbar\omega$, and the phonon density of states, $D_p(\omega)$, Eq. (1) can be rewritten in the energy form [38]:

$$\mathbf{v}_{\omega,p}\cdot\nabla e_{\omega,p,\hat{\mathbf{s}}}=\frac{e^0_{\omega,p}-e_{\omega,p,\hat{\mathbf{s}}}}{\tau_{\omega,p}}+\dot{q}_{\omega,p}. \tag{2}$$

Here, $e_{\omega,p,\hat{\mathbf{s}}}=e(\mathbf{r},\hat{\mathbf{s}},\omega,p)=f(\mathbf{r},\hat{\mathbf{s}},\omega,p)\hbar\omega D_p(\omega)$ denotes the volumetric phonon energy density, which is generally represented by the equivalent phonon temperature [21,38,44]. $e^0_{\omega,p}$ is the corresponding phonon energy density at the equilibrium state that follows the Bose-Einstein distribution. $e^0_{\omega,p}$ is characterized by the lattice temperature, T_{lattice}, which is the common equilibrium temperature that all phonons interact with [17,40] (detailed description is provided in Appendix A). $\tau_{\omega,p}$ is the phonon-relaxation time, which is the average time between two subsequent phonon-phonon scattering events [45]. $\dot{q}_{\omega,p}$ is the volumetric heat generation associated with the phonon mode.

As mentioned earlier, in a hotspot, the heat-generation term represents phonons excited through the electron-phonon scattering process. Some phonon modes strongly scatter with electrons and gain more energy than other modes, leading to selective phonon excitation, which directly leads to differences in phonon energy density. This is the first origin of phonon nonequilibrium, which has been partially addressed in some previous works [17,46]. On the other hand, the phonon-transport term, $\mathbf{v}_{\omega,p}\cdot\nabla e_{\omega,p,\hat{\mathbf{s}}}$, and the phonon-phonon scattering term, $(e^0_{\omega,p}-e_{\omega,p,s})/\tau_{\omega,p}$, govern the transport process of excited phonons. The phonon MFP, $\Lambda_{\omega,p}=v_{\omega,p}\tau_{\omega,p}$, can be used to describe phonon-transport characteristics, where the smaller group velocity and smaller relaxation time lead to a smaller phonon MFP. Phonons with larger MFPs reach the ballistic transport regime and transfer energy from the hotspot more efficiently, while small MFP phonons transfer energy less efficiently and preferentially to scatter with other phonons. This also indicates that different phonons can have different phonon energy densities. This is the second origin of phonon nonequilibrium. When the scale of the hotspot is not much larger than the phonon

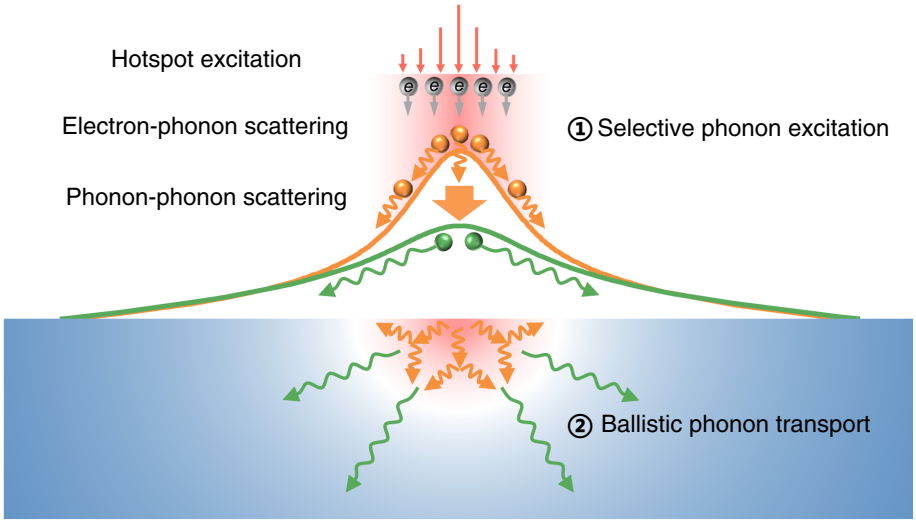

FIG. 1. Illustration of two effects that induce phonon nonequilibrium. Selective excitation is caused by the selective electron-phonon interaction in the hotspot, where some phonon modes usually gain the most energy from electrons (yellow spheres) and some phonon modes (green spheres) gain much less energy from other phonons through phonon-phonon scattering. Ballistic phonon transport refers to the difference in heat-transfer efficiency of phonons with different MFPs, where phonons with MFPs comparable to or even larger than the scale of the hotspot (green spheres) reach the ballistic transport regime.

MFP, phonon transport reaches the ballistic regime and the ballistic transport effect must be considered.

Figure 1 illustrates the phonon nonequilibrium induced by the two effects discussed above, namely, *selective phonon excitation* and *ballistic phonon transport*. We refer to these effects as selective excitation and ballistic transport in subsequent discussions. Generally, phonons with high frequency and low momentum obtain most energy from electrons and usually have small MFPs, while other phonons gaining less energy from electrons have relatively large MFPs [13,15]. Therefore, both selective excitation and ballistic transport, which are inherently included in Eq. (2), should be considered for thermal transport near a nanoscale hotspot in practical applications.

However, previous studies on thermal transport near a nanoscale hotspot have made some simplifications [17,29,30,32,33,46]. For example, if one neglects selective excitation, one basically assumes that the energy, $\dot{q}_{\omega,p}$, gained from the electrons for each phonon mode in Eq. (2) is proportional to its specific heat, $C_{\omega,p}$ [29,30,32], and therefore, no phonon nonequilibrium is introduced by heat generation (see Appendix A for details):

$$\dot{q}_{\omega,p} = \frac{C_{\omega,p}}{C}\dot{q}, \tag{3}$$

where C is the total volumetric heat capacity and $\dot{q}$ is the total heat generation of all phonon modes in the same direction.

Another simplification is to neglect ballistic transport [17,33,46]. In this case, phonon transport is assumed to be pure diffusion, and therefore, the phonon-transport term in Eq. (2) is replaced by a diffusion term. The governing equation becomes

$$\nabla(\kappa_{\omega,p}\nabla T_{\omega,p}) + \frac{C_{\omega,p}}{\tau_{\omega,p}}(T_{\text{lattice}} - T_{\omega,p}) + \int \dot{q}_{\omega,p}\, d\Omega' = 0, \tag{4}$$

where $T_{\omega,p}$ is the temperature of phonons with frequency ω and polarization p. $\kappa_{\omega,p}$ denotes the thermal conductivity. Ω' is the control angle. Here, the second term is the phonon-phonon scattering term and describes the energy exchange between different phonons due to phonon-phonon scattering processes. Equation (4) is also known as the multitemperature model (MTM) [17] (detailed equations are available in Appendix A).

Furthermore, if both selective excitation and ballistic transport are neglected, then local thermal equilibrium is assumed and the local temperature can be well defined. The governing equation becomes the conventional heat-diffusion equation:

$$\nabla(\kappa\nabla T) + \int \dot{q}\, d\Omega' = 0. \tag{5}$$

This equation is usually used in experimental analyses [35,42]. Table I compares the four different approaches for modeling thermal transport near nanoscale hotspots.

B. Nonequilibrium phonon transport near nanoscale hotspots

After analyzing the two effects that induce phonon nonequilibrium, we aim to understand nonequilibrium

TABLE I. Comparison of four different approaches for modeling thermal transport near nanoscale hotspots.

Approach	Selective excitation	Ballistic transport	Governing equation
BTE with selective excitation	Yes	Yes	Eq. (2)
BTE without selective excitation	No	Yes	Eq. (3)
MTM with selective excitation	Yes	No	Eq. (4)
Heat-diffusion equation	No	No	Eq. (5)

phonon transport near nanoscale hotspots by characterizing both effects. Here, we consider a model of a 1D system with length L and thermalizing boundary conditions T_0 at the two ends [47]. Figure 2(a) shows a nanoscale hotspot with heat generation following the Gaussian distribution and a radius of r_0 [35,48] located at the midpoint of the system. Considering that the boundaries also introduce phonon nonequilibrium [49], the length of the 1D system is set to be large enough to avoid the effect of boundaries ($r_0/L \approx 0.01$). We assume that there are only two phonon modes with various transport directions, and the two phonon modes are set to be the same, except for the phonon MFP Λ_j, where j is the index of the phonon mode. The ratio of the phonon MFP Λ_j to the hotspot radius, r_0, gives the Knudsen number, $\mathrm{Kn}_j = \Lambda_j/r_0$ [50]. To reveal the effect of ballistic transport on phonon nonequilibrium, we set one ballistic mode with a Knudsen number of 4 and one diffusive mode with a Knudsen number of 0.5 [50]. Different Knudsen numbers when applying hotspots with different radii r_0 are discussed later in this section. The diffusive phonon mode is assumed to gain all energy under selective excitation. The four approaches for modeling thermal transport near nanoscale hotspots, as listed in Table I, are numerically solved [51], and detailed numerical treatment is available in Appendix A.

Figure 2(b) compares the calculated phonon temperatures of the two phonons from the phonon BTE with selective excitation when considering both effects (solid lines) and the MTM with selective excitation for only the selective excitation effect (dashed lines). The dimensionless position is $x^* = 2r/L$, where r is the distance to the center of the hotspot. The dimensional temperature is defined as $T^* = (T - T_0)/(T_{\max} - T_0)$, where $T_{\max}$ is the maximum temperature. We note that the phonon

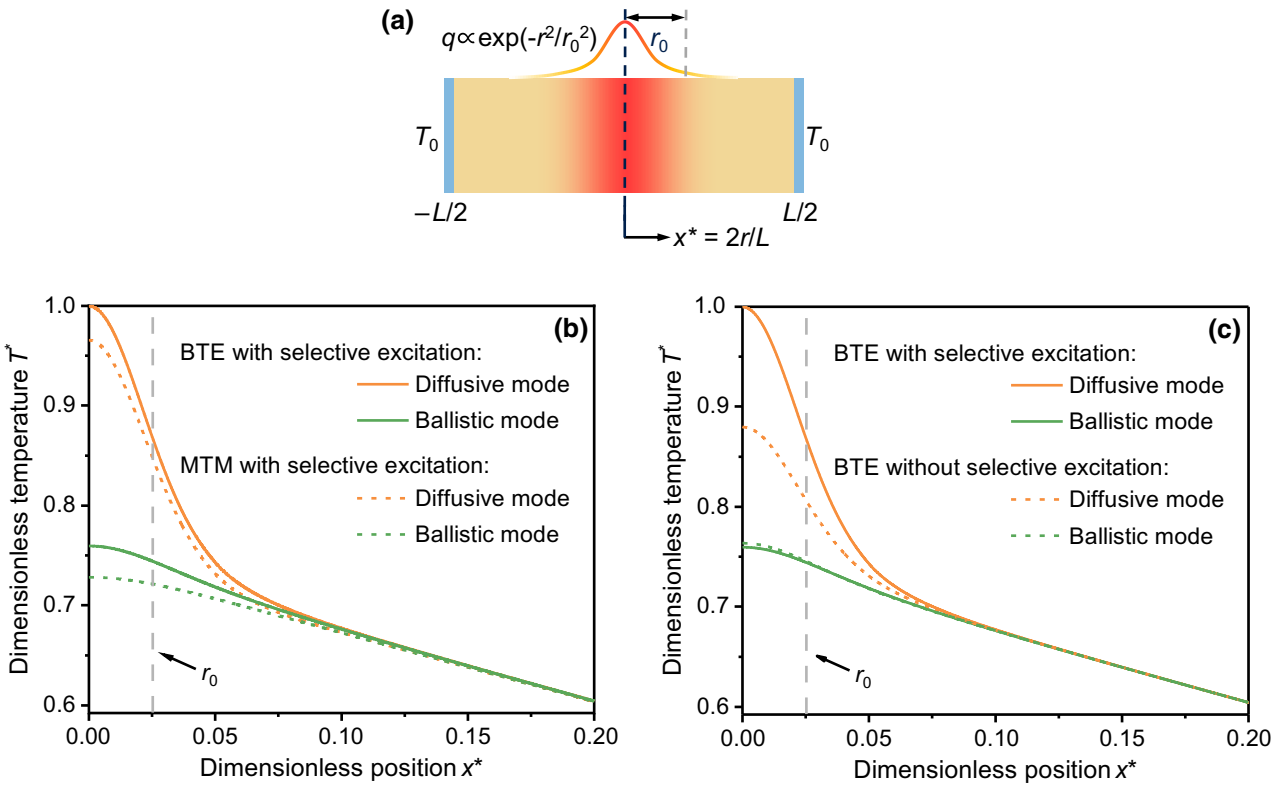

FIG. 2. (a) Simulation domain of a 1D system. Hotspot with a radius of r_0, the heat generation of which follows the Gaussian distribution, is located in the middle of the system. (b) Dimensionless phonon temperature, $T^* = (T - T_0)/(T_{\max} - T_0)$, of the two phonon modes versus the dimensionless position, $x^* = 2r/L$, calculated from the phonon BTE with selective excitation (solid lines) and the MTM with selective excitation (dashed lines). (c) Dimensionless phonon temperature calculated from the phonon BTE with selective excitation [solid lines, same as in (b)] and without selective excitation (dashed lines).

does not actually have a well-defined temperature under the nonequilibrium condition [8,40]. Here, just for a better understanding, we follow convention and define the local phonon temperature based on the distribution function, which is a representation of phonon energy density at a location [40] (see Appendix A for details). It shows that selective excitation directly leads to phonon nonequilibrium, as illustrated by the dashed lines, where the diffusive phonon has a much higher temperature than the ballistic phonon. When further considering ballistic transport, both phonon temperatures increase, as shown by the solid lines. This is because scattering events are rare for ballistic transport, making it more difficult to take thermal energy away from the hotspot [18,19]. Figure 2(c) compares the calculated phonon temperatures of the two phonons from the phonon BTE with selective excitation [solid lines, the same as in Fig. 2(b)] and without selective excitation (dashed lines). As mentioned earlier, the two phonons gain the same amount of energy from the hotspot, when neglecting selective excitation, and no phonon nonequilibrium is induced by heat generation (see Appendix A for details). The obvious phonon nonequilibrium observed in Fig. 2(c) (dashed lines) is induced purely by the ballistic transport effect. Phonons with large MFPs are more capable of transferring energy outwards from the hotspot, leading to phonon nonequilibrium. Further consideration of selective excitation can lead to greater phonon nonequilibrium, as shown by solid lines.

After characterizing phonon nonequilibrium induced by both effects, we also calculate the lattice temperature to analyze the effective thermal conductivity of thermal transport near nanoscale hotspots; this was of wide interest in previous studies [19,20,26,27]. The lattice temperature is the temperature of the scattering lattice reservoir that all phonons interact with and represents the average phonon temperature [40] (see Appendix A for details). Figure 3(a) shows the calculated lattice temperature from the four approaches listed in Table I when considering both effects, only the selective excitation effect, only the ballistic transport effect, and neglecting both effects. It shows that temperatures calculated from both the MTM with selective excitation and the phonon BTE without selective excitation are higher than that predicted by the heat-diffusion equation. This indicates that both selective excitation and ballistic transport lead to a higher temperature rise, i.e., lower effective thermal conductivity than the bulk thermal conductivity, κ_{bulk}. For the phonon BTE with selective excitation, an even higher temperature rise and lower effective thermal conductivity are introduced by both effects. We also investigate the effective thermal conductivity, κ_{eff}, for nanoscale hotspots with different radii r_0, as shown in Fig. 3(b), since it is common to apply different sizes of hotspots in practical applications [52,53]. Here, the inverse Knudsen number is the ratio of r_0 to the average MFP of the two phonons [54]. The effective thermal conductivity is determined by fitting the temperature rise in the hotspot with the heat-diffusion equation [17,50]. It shows that the effective thermal conductivities calculated from the phonon BTE with selective excitation, the MTM with selective excitation, and the phonon BTE without selective excitation are much lower than the bulk thermal conductivity in the heat-diffusion equation, which has contributions from both selective excitation and ballistic transport. Meanwhile, the effective thermal conductivity calculated from the MTM with selective excitation is lower than that predicted by the phonon BTE without selective excitation, which sharply decreases as the hotspot shrinks. This indicates that selective excitation contributes more

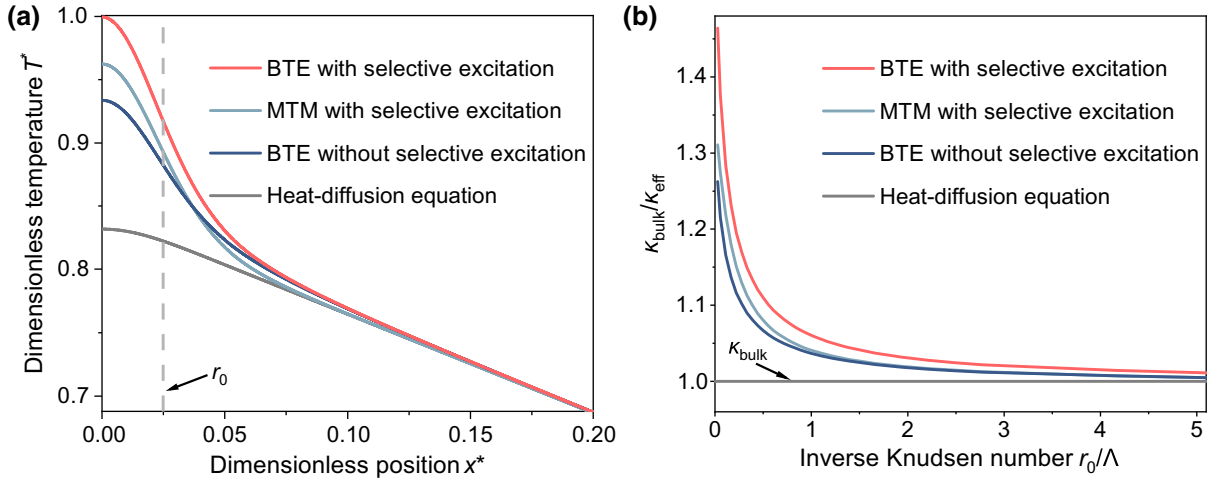

FIG. 3. (a) Dimensionless temperature, $T^* = (T - T_0)/(T_{\max} - T_0)$, versus dimensionless position, $x^* = 2r/L$, calculated from different approaches (same r_0 as in Fig. 2). (b) Ratio of bulk thermal conductivity to effective thermal conductivity, $\kappa_{\text{bulk}}/\kappa_{\text{eff}}$, versus the inverse Knudsen number, r_0/Λ, calculated from different approaches when applying hotspots with different radii r_0.

than ballistic transport to the low effective thermal conductivity, while ballistic transport becomes increasingly important for small hotspots. In addition, as the radius of the hotspot increases, the effective thermal conductivity decreases to the bulk thermal conductivity for different approaches. This is because the larger radius leads to more frequent phonon-phonon scattering near the hotspot where phonon transport becomes diffusive. Meanwhile, the frequent phonon-phonon scattering also results in sufficient energy exchange between different phonons, which reduces the difference in phonon temperatures. Therefore, phonon nonequilibrium induced by both effects vanishes in large hotspots and thermal transport approaches the diffusive regime. When the hotspot radius is greater than 5 times the average phonon MFP, both effects can be neglected and the heat-diffusion equation is valid.

III. QUANTITATIVE STUDY

In this section, after analyzing the mechanism of nonequilibrium phonon transport near nanoscale hotspots, we aim to further quantitatively study thermal transport near nanoscale hotspots in practical applications based on two case studies, i.e., laser heating of spots in Raman spectroscopy and Joule heating of spots in silicon bulk fin FETs.

A. Nanoscale laser heating of a spot in Raman spectroscopy

As a widely used experimental technique to measure thermal conductivity and other thermal properties of nanomaterials, Raman spectroscopy is based on the local thermal equilibrium assumption, which is inaccurate when Raman laser heating of nanoscale spots is applied [35,55–57]. When measuring the thermal conductivity, Raman spectroscopy probes the average optical phonon (OP) temperature, T_{OP}, and uses T_{OP} to determine the thermal conductivity, κ_{Raman}, according to the heat-diffusion equation: $\kappa_{Raman}\nabla^2 T_{OP} + Q_{laser} = 0$ [35]. Vallabhaneni *et al.* [17] considered selective excitation and found significantly underestimated thermal conductivity in Raman measurements for suspended single-layer graphene (SLG) compared with the intrinsic value, $\kappa_{intrinsic}$, due to phonon nonequilibrium. However, based on our earlier discussion of Fig. 3, phonon nonequilibrium near nanoscale hotspots is also determined by ballistic transport and varies with different hotspot radii, thus leading to further underestimated thermal conductivity in Raman measurements.

To quantitatively calculate the Raman-measured thermal conductivity, κ_{Raman}, we perform the phonon BTE calculations for 10×10-μm^2 suspended SLG with four thermalizing boundaries of 300 K, approximating the Raman experiment setup shown in Fig. 4(a) [17,46]. Thermal properties of the SLG needed to solve the phonon BTE are extracted from Ref. [46]. The phonon MFP and percentage of excited energy obtained by different phonons from the laser-heated spot are listed in Table II. It shows that longitudinal optical (LO) phonons and transverse optical (TO) phonons have small MFPs and gain most of the excited energy, while acoustic phonons with large MFPs gain little energy, which is consistent with our analysis in Sec. II. The calculated dimensionless phonon-temperature rise, $\Delta T_j/\Delta T_{lattice}$, within the laser-heated hotspot with a radius of 0.5 μm calculated from the phonon BTE with selective excitation is also given in Table II as an

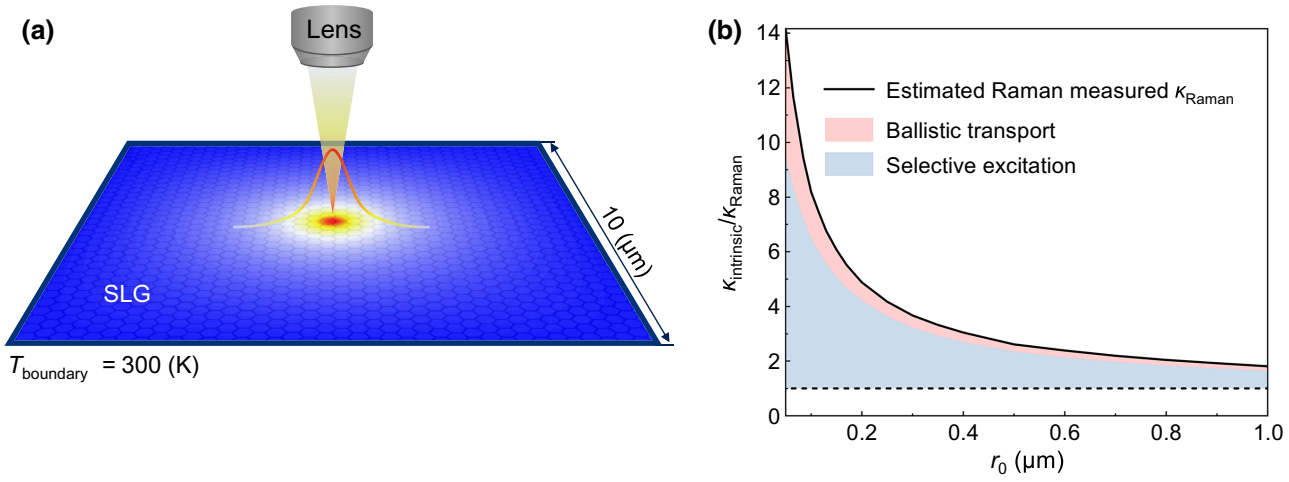

FIG. 4. (a) Schematic of a 10×10-μm^2 suspended SLG approximating the Raman experiment setup. (b) Discrepancy between Raman-measured thermal conductivity, κ_{Raman}, and intrinsic thermal conductivity, $\kappa_{intrinsic}$, when applying laser-heated spots with different radii r_0. Solid line represents κ_{Raman} evaluated by the phonon BTE with selective excitation. Red and blue areas represent contributions of ballistic transport and selective excitation to the underestimated Raman-measured thermal conductivity, respectively.

TABLE II. Thermal properties of the SLG and the dimensionless phonon-temperature rise within the laser-heated spot.

	LA	TA	ZA	LO	TO	ZO
MFP (nm) [46]	802	191.6	1700	81.7	109.5	318.4
% of excited energy [46]	2.94	0.03	0	17.64	79.39	0
$\Delta T_j/\Delta T_{\text{lattice}}$	0.66	0.93	0.44	1.18	2.50	0.85

example. Here, ΔT_j and $\Delta T_{\text{lattice}}$ are the spatially averaged phonon-temperature rise and lattice-temperature rise within the hotspot [35], where subscript j represents the index of the phonon. Clear phonon-temperature nonequilibrium between optical phonons and acoustic phonons is observed in the SLG. When applying laser-heated spots with different radii, the discrepancy between calculated κ_{Raman} and $\kappa_{\text{intrinsic}}$ caused by the phonon nonequilibrium is shown in Fig. 4(b). The solid line plots the ratio of $\kappa_{\text{intrinsic}}$ to κ_{Raman} which is estimated by the average optical phonon temperature calculated from the phonon BTE with selective excitation, and the dashed line represents the intrinsic thermal conductivity. These results show that the measured thermal conductivity in the Raman experiments is already underestimated when the radius of the laser-heated spot is reduced to 1 μm (by a factor of 1.81). This underestimation of thermal conductivity significantly increases as the laser-heated spots shrink. To further distinguish the contributions of both effects to the underestimated thermal conductivity, we also resolve the MTM with selective excitation and compare it with the phonon BTE results. The blue areas and red areas in Fig. 4(b) show the contributions of selective excitation and ballistic transport, respectively. This indicates that the underestimation of thermal conductivity mainly originates from selective excitation. The contribution from ballistic transport becomes more important for smaller laser-heated spots. For a laser-heated spot with a radius of 0.5 μm, our results show that the measured thermal conductivity in Raman experiments is underestimated by a factor of 2.61, of which 84% is contributed by selective excitation and 16% is contributed by ballistic transport.

We note that this experimental error in Raman thermal conductivity measurements caused by nonequilibrium phonon transport near nanoscale hotspots is dependent on the size of the applied laser-heated spot [52,53]. One can roughly neglect both effects and apply the heat-diffusion equation when the hotspot radius is greater than 5 times the average phonon MFP, according to Fig. 3(b). Specific experimental errors for SLG, the average phonon MFP of which is 927 nm [46], can be estimated from Fig. 4(b). Our findings provide guidance for evaluating and minimizing the experimental errors in Raman measurements by regulating both selective excitation and ballistic transport.

B. Nanoscale Joule heating of a spot in silicon bulk fin FETs

As modern commercial transistors scale down to tens of nanometers, the traditional planar MOSFET is replaced by the fin FET for further miniaturization [58]. The generated Joule heating spot near the channel-drain junction of a working fin FET caused by the self-heating effect has an even smaller size of several nanometers [59]. As discussed earlier, this nanoscale Joule heating spot can lead to strong phonon nonequilibrium and decreased effective thermal conductivity, which can pose severe challenges for the thermal management of electronic devices [22,60].

To quantitatively analyze thermal transport in transistors, we take a 22-nm technology-node silicon bulk fin FET designed previously [59] as the study case, which is shown in Fig. 5(a). Detailed structures and device parameters can be found in Appendix B and Ref. [59]. A Joule heating spot with a height, H_{Joule}, of 10 nm and a width, W_{Joule}, of 5 nm near the channel-drain junction is assumed to be reasonable, according to electrical simulation results of this fin FET in previous studies [59]. The simulation is conducted in the two-dimensional plane shown by the black dashed line in Fig. 5(a). The left and right boundaries are set as the specularly reflecting boundary condition, which is an adiabatic boundary condition for symmetrical structures [61]. The top boundary is set as the diffusely reflecting boundary condition, which is another type of adiabatic boundary condition for the surface of the semiconductor or the dioxide layer [62,63]; the bottom substrate is the heat sink and is set as the thermalizing boundary of 300 K. Thermal properties for silicon needed to solve the phonon BTE are obtained from first-principles calculations [64,65]. The percentage of excited energy obtained by different phonons from the Joule heating spot is extracted from Ref. [16], as listed in Table III.

The calculated dimensionless phonon-temperature rises, $\Delta T_j/\Delta T_{\text{lattice}}$, within the Joule heating hotspot from the phonon BTE with selective excitation are also given in Table III, which shows clear phonon-temperature nonequilibrium between optical phonons and acoustic phonons. Figures 5(b) and 5(c) show the temperature distribution calculated from the heat-diffusion equation and the phonon BTE with selective excitation, respectively. This illustrates that a much higher and localized temperature rise is induced by phonon nonequilibrium due to both selective excitation and ballistic transport. This implies a significant additional thermal resistance in the silicon fin FET and inefficient heat dissipation. Using the average temperature rise within the Joule heating spot, we also evaluate the effective thermal conductivity of the transistor, which equals 12 W/mK and is much lower than the bulk silicon thermal conductivity of 155 W/mK. This means that the effective thermal conductivity decreases by nearly 13 times, of which 54% is contributed by selective excitation and 46% by ballistic transport. Here, ballistic

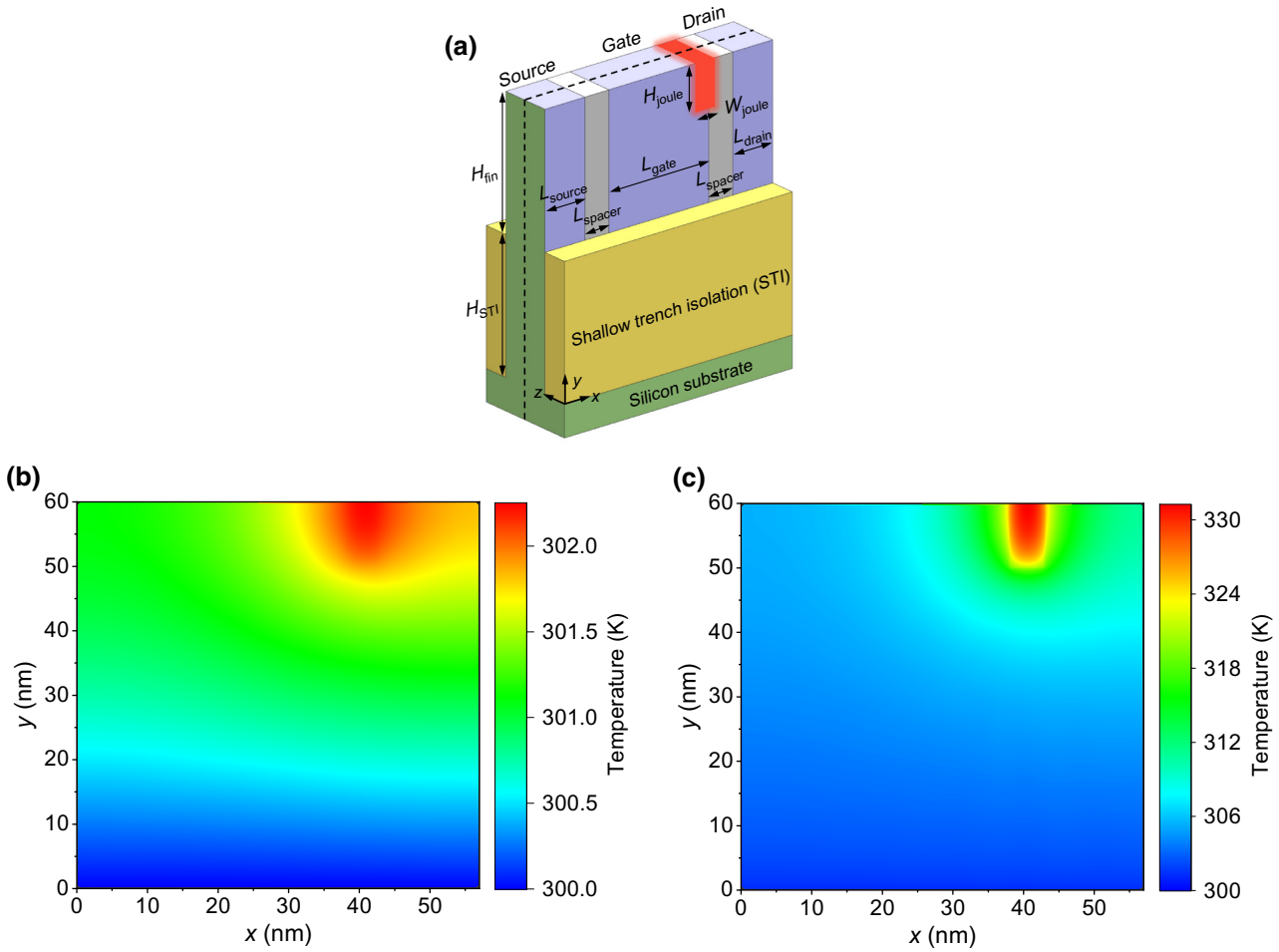

FIG. 5. (a) Schematic of the silicon bulk fin FET with a gate length, L_{gate}, of 25 nm [57]. Temperature distribution in the two-dimensional plane indicated by the black dashed line in (a) calculated by (b) the heat-diffusion equation and (c) the phonon BTE with selective excitation.

transport contributes almost equally to the decreased effective thermal conductivity as selective excitation due to the extremely small size of the Joule heating spot. As modern commercial transistors scale down to 14- and even 7-nm technology nodes, the effective thermal conductivity can further decrease and cause higher thermal resistance, as ballistic transport within a single transistor becomes increasingly important for the entire junction-to-package-level thermal management of nanoelectronics [5].

TABLE III. Thermal properties of silicon and the dimensionless phonon-temperature rise within the Joule heating spot.

	TA1	TA2	LA	LO	TO1	TO2
MFP (nm)	171.1	147.3	108.8	31.5	3.4	4.0
% of excited energy [16]	2.0	2.4	16.0	59.0	10.5	10.1
$\Delta T_j/\Delta T_{lattice}$	0.22	0.23	0.40	1.29	1.08	1.09

IV. CONCLUSION

We present a quantitative study of nonequilibrium phonon transport near nanoscale hotspots based on the phonon BTE. We find that effective thermal conductivity near nanoscale hotspots decreases with shrinking hotspot size due to nonequilibrium phonon transport. Two effects that induce this phonon nonequilibrium are revealed, i.e., selective phonon excitation and ballistic phonon transport. Taking nanoscale hotspots in 1D systems as prototypes, we distinguish between phonon nonequilibrium resulting from both effects by comparing four different approaches to model phonon transport. Ballistic phonon transport is shown to directly cause phonon nonequilibrium, and nonequilibrium can be even larger when selective phonon excitation exists. We also find that phonon nonequilibrium is primarily contributed to by selective phonon excitation, but the contribution from ballistic phonon transport is also important for smaller hotspots. Meanwhile, when the hotspot radius is greater than 5 times the average phonon mean free path, both effects are roughly negligible, and

the heat-diffusion equation becomes valid. Furthermore, we also show that nanoscale-hotspot-induced phonon nonequilibrium can lead to significantly underestimated thermal conductivity measured in Raman experiments and decreased effective thermal conductivity in nanoscale transistors. Specifically, when applying a laser-heated spot with a radius of 0.5 μm on suspended SLG, the thermal conductivity measured by the Raman experiments is underestimated by a factor of 2.61. This measurement error in Raman experiments further increases as the laser spot size decreases. For a 22-nm technology-node silicon fin FET, the effective thermal conductivity decreases by nearly 13 times. This thermal performance deterioration in transistors is expected to become more severe at 14- and 7-nm technology nodes, where phonon nonequilibrium can pose greater challenges for the entire junction-to-package-level thermal management of electronics.

Finally, we would like to mention that nonequilibrium phonon transport is also important under transient conditions, where the timescale is comparable to the phonon-relaxation time, as in time-domain thermoreflectance experiments [3], and affects thermal transport across interfaces [2]. In these cases, the transient effect and differences in phonon transmittance across interfaces may also induce phonon nonequilibrium. Therefore, it is worth further extending the theoretical framework of the phonon BTE to investigate nonequilibrium phonon transport under transient conditions and across interfaces in the future.

ACKNOWLEDGMENTS

J.X., Y.H., and H.B. acknowledge support by the National Natural Science Foundation of China (Grant No. 52122606). Simulations are performed on the π 2.0 cluster supported by the Center for High Performance Computing at Shanghai Jiao Tong University.

APPENDIX A: PHONON BTE AND NUMERICAL METHODS

First, we present brief derivations of the theoretical formula for the four approaches to model thermal transport near nanoscale hotspots, as shown in Sec. II of the main text. Starting from the phonon BTE with the energy form, as given in Eq. (2), i.e.,

$$\mathbf{v}_{\omega,p}\cdot\nabla e_{\omega,p,\hat{\mathbf{s}}}=\frac{e^0_{\omega,p}-e_{\omega,p,\hat{\mathbf{s}}}}{\tau_{\omega,p}}+\dot{q}_{\omega,p}. \tag{A1}$$

The temperature of phonons with frequency ω and polarization p is given by

$$C_{\omega,p}(T_{\omega,p}-T_{\mathrm{ref}})=\int_{\Omega'}e_{\omega,p,\hat{\mathbf{s}}}d\Omega', \tag{A2}$$

where T_{ref} denotes the reference temperature, and the integral over angular space at the left-hand side of Eq. (A2) represents the energy density of phonons with frequency ω and polarization p [40]. Note that, since the local thermal equilibrium assumption is invalid, the phonon temperature, $T_{\omega,p}$, is not the thermodynamic temperature. Instead, it is merely a representation of phonon energy density at a location; this is commonly used in many other works [39,40,47].

When neglecting selective excitation in the phonon BTE, the volumetric heat generation of each phonon mode, $\dot{q}_{\omega,p}$, is proportional to its specific heat [29,30,32], i.e., $\dot{q}_{\omega,p}=(C_{\omega,p}/C)\dot{q}$, as also given in Eq. (3). According to Eq. (A2), this implies that temperature rises, $T_{\omega,p}-T_{\mathrm{ref}}$, caused by the heat generation of all phonons are the same, i.e., no phonon-temperature nonequilibrium is introduced by heat generation. Therefore, in this case, the phonon BTE excludes the selective excitation effect and includes only the ballistic transport effect.

On the other hand, when neglecting ballistic transport in the phonon BTE, we integrate Eq. (A1) over the angular space,

$$\nabla\cdot\mathbf{Q}_{\omega,p}=\frac{C_{\omega,p}}{\tau_{\omega,p}}(T_{\mathrm{lattice}}-T_{\omega,p})+\int_{\Omega'}\dot{q}_{\omega,p}d\Omega', \tag{A3}$$

where $\mathbf{Q}_{\omega,p}$ is the heat-flux vector for phonons with frequency ω and polarization p, which equals

$$\mathbf{Q}_{\omega,p}=\int_{\Omega'}v_{\omega,p}e_{\omega,p,\hat{\mathbf{s}}}\hat{\mathbf{s}}d\Omega'. \tag{A4}$$

When ignoring ballistic transport, the phonon energy density, $e_{\omega,p,\hat{\mathbf{s}}}$, can be written as the angular-averaged energy density, $\bar{e}_{\omega,p}$, plus a small perturbation, $\Phi_{\omega,p,\hat{\mathbf{s}}}$ [40]:

$$e_{\omega,p,\hat{\mathbf{s}}}=\bar{e}_{\omega,p}+\Phi_{\omega,p,\hat{\mathbf{s}}}, \tag{A5}$$

where the angular-averaged energy density, $\bar{e}_{\omega,p}$, is

$$\bar{e}_{\omega,p}=\frac{\int_{\Omega'}e_{\omega,p,\hat{\mathbf{s}}}d\Omega'}{\Omega}, \tag{A6}$$

where Ω is the total solid angle. Inserting Eq. (A5) into Eq. (A1) and assuming the divergence of $v_{\omega,p}\Phi_{\omega,p,\hat{\mathbf{s}}}$ to be much smaller than the divergence of $v_{\omega,p}\bar{e}_{\omega,p}$, we have

$$\Phi_{\omega,p,\hat{\mathbf{s}}}=\frac{C_{\omega,p}}{\Omega}[(T_{\mathrm{lattice}}-T_{\omega,p})-v_{\omega,p}\tau_{\omega,p}\nabla\cdot(\hat{\mathbf{s}}T_{\omega,p})]+\tau_{\omega,p}\frac{\int_{\Omega'}\dot{q}_{\omega,p}d\Omega'}{\Omega}. \tag{A7}$$

Combining Eqs. (A5) and (A7), we have

$$e_{\omega,p,\hat{\mathbf{s}}}=e^0_{\omega,p}-\frac{C_{\omega,p}v_{\omega,p}\tau_{\omega,p}}{\Omega}\nabla\cdot(\hat{\mathbf{s}}T_{\omega,p})+\tau_{\omega,p}\frac{\int_{\Omega'}\dot{q}_{\omega,p}d\Omega'}{\Omega}. \tag{A8}$$

Based on the isotropic assumption [47], $e^0_{\omega,p}$ and $\int_{\Omega'}\dot{q}_{\omega,p}d\Omega'$ are angle independent. Inserting Eq. (A8) into

Eq. (A4), we have

$$\mathbf{Q}_{\omega,p} = -\frac{C_{\omega,p} v_{\omega,p}^2 \tau_{\omega,p}}{\Omega} \int_{\Omega'} \nabla \cdot (\hat{\mathbf{s}} T_{\omega,p}) \hat{\mathbf{s}} d\Omega', \tag{A9}$$

which yields

$$\mathbf{Q}_{\omega,p} = -\kappa_{\omega,p} \nabla T_{\omega,p}, \tag{A10}$$

where $\kappa_{\omega,p}$ is the thermal conductivity associated with phonons with frequency ω and polarization p. Inserting Eq. (A10) into Eq. (A3), we obtain

$$\nabla(\kappa_{\omega,p} \nabla T) + \frac{C_{\omega,p}}{\tau_{\omega,p}}(T_{\text{lattice}} - T_{\omega,p}) + \int_{\Omega'} \dot{q}_{\omega,p} d\Omega' = 0. \tag{A11}$$

Equation (A11) is Eq. (4) given in the main text, which implies that selective excitation directly induces different phonon temperatures, $T_{\omega,p}$. Equation (A11) is also known as the multitemperature model [17]. The derivation of Eqs. (A3)–(A11) can also be found in Ref. [40]. When ignoring selective excitation, Eq. (A11) can be further reduced to the heat-diffusion equation, as given in Eq. (5).We note that the thermalizing boundary condition cannot be directly applied in Eq. (A11), where an equivalent boundary condition is applied instead [40]. This difference in boundary conditions results in the temperatures calculated when considering different effects of phonon nonequilibrium still not merging away from the hotspot in 1D systems. To clearly show phonon nonequilibrium near the hotspots, the effect of this difference in boundary conditions on phonon-temperature nonequilibrium is ruled out in Sec. II.

Second, to calculate the phonon temperature, we need to numerically solve phonon BTE Eq. (A1) with the energy-conservation rule [26]:

$$\int_{\Omega} \sum_p \int_{\omega_{\min}}^{\omega_{\max}} \frac{e^0_{\omega,p} - e_{\omega,p,\hat{\mathbf{s}}}}{\tau_{\omega,p}} d\omega' d\Omega' = 0. \tag{A12}$$

Then, the lattice temperature can be determined by

$$T_L = \frac{\int_{\Omega} \sum_p \int_{\omega_{\min}}^{\omega_{\max}} \frac{e_{\omega,p,\hat{\mathbf{s}}}}{\tau_{\omega,p}} d\omega' d\Omega'}{\sum_p \int_{\omega_{\min}}^{\omega_{\max}} \frac{C_{\omega,p}}{\tau_{\omega,p}} d\omega'}. \tag{A13}$$

The input physical properties $v_{\omega,p}$, $C_{\omega,p}$, $\tau_{\omega,p}$, and $\dot{q}_{\omega,p}$ are needed to solve the phonon BTE. For SLG studied in Sec. III A, the input physical properties are extracted from Ref. [46] and are computed using first-principles calculations. For silicon studied in Sec. III B, $v_{\omega,p}$, $C_{\omega,p}$, and $\tau_{\omega,p}$ are also obtained from first-principles calculations [64–67], and information on selective phonon excitation in the Joule heating spot is extracted from Ref. [16]. Therefore, different phonons are already differentiated at the mode level. After obtaining the inputs, we use deterministic methods to numerically solve the phonon BTE. We apply the discrete ordinates method to divide the angular space, and the finite-volume method is employed for spatial discretization [40,41,51]. Further numerical details for solving the phonon BTE can be found in previous studies [47,49,51]. After solving the phonon BTE, we obtain the energy density, $e_{\omega,p,\hat{\mathbf{s}}}$, of each phonon and the corresponding phonon energy density, $e^0_{\omega,p}$, at the equilibrium state. Then, the lattice temperature, T_{lattice}, can be calculated using Eq. (A13), and the temperature of different phonons can also be distinguished according to Eq. (A2).

APPENDIX B: DEVICE PARAMETERS OF THE SILICON BULK FIN FET

The device parameters of the silicon bulk fin FET shown in Fig. 5(a) are listed in Table IV.

TABLE IV. Nominal device parameters of the bulk silicon fin FET from Ref. [59].

Parameter	Value (nm)
Gate length, L_{gate}	25
Source (drain) length, L_{source} (L_{drain})	10
Spacer length, L_{spacer}	6
Fin height, H_{fin}	30
Shallow trench isolation depth, H_{STI}	30
Joule heating spot height, H_{Joule}	10
Joule heating spot width, W_{Joule}	5

[1] Y. Yue, X. Chen, and X. Wang, Noncontact sub-10 nm temperature measurement in near-field laser heating, ACS Nano **5**, 4466 (2011).

[2] D. Zhao, X. Qian, X. Gu, S. A. Jajja, and R. Yang, Measurement techniques for thermal conductivity and interfacial thermal conductance of bulk and thin film materials, J. Electron. Packag. **138**, 040802 (2016).

[3] P. Jiang, X. Qian, X. Gu, and R. Yang, Probing anisotropic thermal conductivity of transition metal dichalcogenides MX_2 (M = Mo, W and X = S, Se) using time-domain thermoreflectance, Adv. Mater. **29**, 1701068 (2017).

[4] Y. C. Hua, H. L. Li, and B. Y. Cao, Thermal spreading resistance in ballistic-diffusive regime for GaN HEMTs, IEEE Trans. Electron Devices **66**, 3296 (2019).

[5] R. J. Warzoha, A. A. Wilson, B. F. Donovan, N. Donmezer, A. Giri, P. E. Hopkins, S. Choi, D. Pahinkar, J. Shi, S. Graham, *et al.*, Applications and impacts of nanoscale thermal transport in electronics packaging, J Electron Packag **143**, 020804 (2021).

[6] Y. Zhao, Y. Cai, L. Zhang, B. Li, G. Zhang, and J. T. L. Thong, Thermal transport in 2D semiconductors—considerations for device applications, Adv. Funct. Mater. **30**, 1903929 (2020).

[7] G. M. Vanacore, J. Hu, W. Liang, S. Bietti, S. Sanguinetti, and A. H. Zewail, Diffraction of quantum dots reveals nanoscale ultrafast energy localization, Nano Lett. **14**, 6148 (2014).

[8] D. G. Cahill, W. K. Ford, K. E. Goodson, G. D. Mahan, A. Majumdar, H. J. Maris, R. Merlin, and S. R. Phillpot, Nanoscale thermal transport, J. Appl. Phys. **93**, 793 (2003).

[9] A. Majumdar, Microscale heat conduction in dielectric thin films, J. Heat Transfer **115**, 7 (1993).

[10] B. Vermeersch and N. Mingo, Quasiballistic heat removal from small sources studied from first principles, Phys. Rev. B **97**, 045205 (2018).

[11] G. Chen, Non-Fourier phonon heat conduction at the microscale and nanoscale, Nat. Rev. Phy. **3**, 555 (2021).

[12] E. Pop, R. W. Dutton, and K. E. Goodson, Monte Carlo simulation of Joule heating in bulk and strained silicon, Appl. Phys. Lett. **86**, 082101 (2005).

[13] S. Sadasivam, M. K. Y. Chan, and P. Darancet, Theory of Thermal Relaxation of Electrons in Semiconductors, Phys. Rev. Lett. **119**, 136602 (2017).

[14] E. Minamitani, *Ab initio* analysis for the initial process of Joule heating in semiconductors, Phys. Rev. B **104**, 085202 (2021).

[15] X. Tong and M. Bernardi, Toward precise simulations of the coupled ultrafast dynamics of electrons and atomic vibrations in materials, Phys. Rev. Res. **3**, 023072 (2021).

[16] C. Ni, Z. Aksamija, J. Y. Murthy, and U. Ravaioli, Coupled electro-thermal simulation of MOSFETs, J Comput Electron **11**, 93 (2012).

[17] A. K. Vallabhaneni, D. Singh, H. Bao, J. Murthy, and X. Ruan, Reliability of Raman measurements of thermal conductivity of single-layer graphene due to selective electron-phonon coupling: A first-principles study, Phys. Rev. B **93**, 125432 (2016).

[18] G. Chen, Nonlocal and nonequilibrium heat conduction in the vicinity of nanoparticles, J. Heat Transfer **118**, 539 (1996).

[19] M. E. Siemens, Q. Li, R. Yang, K. A. Nelson, E. H. Anderson, M. M. Murnane, and H. C. Kapteyn, Quasi-ballistic thermal transport from nanoscale interfaces observed using ultrafast coherent soft x-ray beams, Nat. Mater. **9**, 26 (2010).

[20] Y. Hu, L. Zeng, A. J. Minnich, M. S. Dresselhaus, and G. Chen, Spectral mapping of thermal conductivity through nanoscale ballistic transport, Nat. Nanotechnol. **10**, 701 (2015).

[21] S. Sinha, E. Pop, R. W. Dutton, and K. E. Goodson, Non-equilibrium phonon distributions in sub-100 nm silicon transistors, J. Heat Transfer **128**, 638 (2005).

[22] Q. Hao, H. Zhao, Y. Xiao, and M. B. Kronenfeld, Electrothermal studies of GaN-based high electron mobility transistors with improved thermal designs, Int. J. Heat Mass Transfer **116**, 496 (2018).

[23] S. Das, A. Sebastian, E. Pop, C. J. McClellan, A. D. Franklin, T. Grasser, T. Knobloch, Y. Illarionov, A. V. Penumatcha, J. Appenzeller, *et al.*, Transistors based on two-dimensional materials for future integrated circuits, Nat. Electron. **4**, 786 (2021).

[24] K. M. Hoogeboom-Pot, J. N. Hernandez-Charpak, X. Gu, T. D. Frazer, E. H. Anderson, W. Chao, R. W. Falcone, R. Yang, M. M. Murnane, H. C. Kapteyn, *et al.*, A new regime of nanoscale thermal transport: Collective diffusion increases dissipation efficiency, Proc. Natl. Acad. Sci. U. S. A. **112**, 4846 (2015).

[25] X. Chen, C. Hua, H. Zhang, N. K. Ravichandran, and A. J. Minnich, Quasiballistic Thermal Transport from Nanoscale Heaters and the Role of the Spatial Frequency, Phys. Rev. Appl. **10**, 054068 (2018).

[26] T. D. Frazer, J. L. Knobloch, K. M. Hoogeboom-Pot, D. Nardi, W. Chao, R. W. Falcone, M. M. Murnane, H. C. Kapteyn, and J. N. Hernandez-Charpak, Engineering Nanoscale Thermal Transport: Size- and Spacing-Dependent Cooling of Nanostructures, Phys. Rev. Appl. **11**, 024042 (2019).

[27] H. Honarvar, J. L. Knobloch, T. D. Frazer, B. Abad, B. McBennett, M. I. Hussein, H. C. Kapteyn, M. M. Murnane, and J. N. Hernandez-Charpak, Directional thermal channeling: A phenomenon triggered by tight packing of heat sources, Proc. Natl. Acad. Sci. U. S. A. **118**, e2109056118 (2021).

[28] C. Hua and A. J. Minnich, Analytical Green's function of the multidimensional frequency-dependent phonon Boltzmann equation, Phys. Rev. B **90**, 214306 (2014).

[29] B. Vermeersch, J. Carrete, N. Mingo, and A. Shakouri, Superdiffusive heat conduction in semiconductor alloys. I. Theoretical foundations, Phys. Rev. B **91**, 085202 (2015).

[30] S. Huberman, V. Chiloyan, R. A. Duncan, L. Zeng, R. Jia, A. A. Maznev, E. A. Fitzgerald, K. A. Nelson, and G. Chen, Unifying first-principles theoretical predictions and experimental measurements of size effects in thermal transport in SiGe alloys, Phys. Rev. Mater. **1**, 054601 (2017).

[31] C. Hua and A. J. Minnich, Heat dissipation in the quasiballistic regime studied using the Boltzmann equation in the spatial frequency domain, Phys. Rev. B **97**, 014307 (2018).

[32] V. Chiloyan, S. Huberman, A. A. Maznev, K. A. Nelson, and G. Chen, Thermal transport exceeding bulk heat conduction due to nonthermal micro/nanoscale phonon populations, Appl. Phys. Lett. **116**, 163102 (2020).

[33] S. Sullivan, A. Vallabhaneni, I. Kholmanov, X. Ruan, J. Murthy, and L. Shi, Optical generation and detection of local nonequilibrium phonons in suspended graphene, Nano Lett. **17**, 2049 (2017).

[34] R. J. Dolleman, G. J. Verbiest, Y. M. Blanter, H. S. J. van der Zant, and P. G. Steeneken, Nonequilibrium thermodynamics of acoustic phonons in suspended graphene, Phys. Rev. Res. **2**, 012058 (2020).

[35] R. Wang, H. Zobeiri, Y. Xie, X. Wang, X. Zhang, and Y. Yue, Distinguishing optical and acoustic phonon temperatures and their energy coupling factor under photon excitation in nm 2D materials, Adv. Sci. **7**, 2000097 (2020).

[36] H. Zobeiri, N. Hunter, R. Wang, T. Wang, and X. Wang, Direct characterization of thermal nonequilibrium between optical and acoustic phonons in graphene paper under photon excitation, Adv. Sci. **8**, 2004712 (2021).

[37] M. Kaviany, *Heat transfer physics* (Cambridge University Press, New York, 2014).

[38] H. Bao, J. Chen, X. Gu, and B. Cao, A review of simulation methods in micro/nanoscale heat conduction, ES Energy Environ. **1**, 16 (2018).

[39] W. Miao and M. Wang, Nonequilibrium effects on the electron-phonon coupling constant in metals, Phys. Rev. B **103**, 125412 (2021).

[40] J. M. Loy, J. Y. Murthy, and D. Singh, A fast hybrid Fourier–Boltzmann transport equation solver for nongray phonon transport, J. Heat Transfer **135**, 011008 (2012).

[41] S. Zahiri, J. Zuo, Y. Shen, and H. Bao, Numerical investigation of ballistic-diffusive heat transfer through a constriction with the Boltzmann transport equation, Appl. Therm. Eng. **141**, 126 (2018).

[42] C. Hua, L. Lindsay, X. Chen, and A. J. Minnich, Generalized Fourier's law for nondiffusive thermal transport: Theory and experiment, Phys. Rev. B **100**, 085203 (2019).

[43] E. Pop, S. Sinha, and K. E. Goodson, Heat generation and transport in nanometer-scale transistors, Proc. IEEE **94**, 1587 (2006).

[44] S. V. J. Narumanchi, J. Y. Murthy, and C. H. Amon, Boltzmann transport equation-based thermal modeling approaches for hotspots in microelectronics, Heat Mass Transf. **42**, 478 (2006).

[45] G. Chen, *Nanoscale energy transport and conversion: a parallel treatment of electrons, molecules, phonons, and photons* (Oxford University Press, New York, 2005).

[46] Z. Lu, A. Vallabhaneni, B. Cao, and X. Ruan, Phonon branch-resolved electron-phonon coupling and the multitemperature model, Phys. Rev. B **98**, 134309 (2018).

[47] Y. Hu, T. Feng, X. Gu, Z. Fan, X. Wang, M. Lundstrom, S. S. Shrestha, and H. Bao, Unification of nonequilibrium molecular dynamics and the mode-resolved phonon Boltzmann equation for thermal transport simulations, Phys. Rev. B **101**, 155308 (2020).

[48] Q.-Y. Li, K. Xia, J. Zhang, Y. Zhang, Q. Li, K. Takahashi, and X. Zhang, Measurement of specific heat and thermal conductivity of supported and suspended graphene by a comprehensive Raman optothermal method, Nanoscale **9**, 10784 (2017).

[49] J. Xu, Y. Hu, X. Ruan, X. Wang, T. Feng, and H. Bao, Nonequilibrium phonon transport induced by finite sizes: Effect of phonon-phonon coupling, Phys. Rev. B **104**, 104310 (2021).

[50] J. Kaiser, T. Feng, J. Maassen, X. Wang, X. Ruan, and M. Lundstrom, Thermal transport at the nanoscale: A Fourier's law vs. phonon Boltzmann equation study, J. Appl. Phys. **121**, 044302 (2017).

[51] Y. Hu, Y. Shen, and H. Bao, Ultra-efficient and parameter-free computation of submicron thermal transport with phonon Boltzmann transport equation, Fundam. Res. (2022).

[52] H. Zobeiri, R. Wang, T. Wang, H. Lin, C. Deng, and X. Wang, Frequency-domain energy transport state-resolved Raman for measuring the thermal conductivity of suspended nm-thick $MoSe_2$, Int. J. Heat Mass Transfer **133**, 1074 (2019).

[53] H. Zobeiri, R. Wang, Q. Zhang, G. Zhu, and X. Wang, Hot carrier transfer and phonon transport in suspended nm WS_2 films, Acta Mater. **175**, 222 (2019).

[54] Y. Hu, Y. Shen, and H. Bao, Optimized phonon band discretization scheme for efficiently solving the nongray Boltzmann transport equation, J. Heat Transfer **144**, 072501 (2022).

[55] W. Cai, A. L. Moore, Y. Zhu, X. Li, S. Chen, L. Shi, and R. S. Ruoff, Thermal transport in suspended and supported monolayer graphene grown by chemical vapor deposition, Nano Lett. **10**, 1645 (2010).

[56] J. H. Seol, I. Jo, A. L. Moore, L. Lindsay, Z. H. Aitken, M. T. Pettes, X. Li, Z. Yao, R. Huang, D. Broido, *et al.*, Two-dimensional phonon transport in supported graphene, Science **328**, 213 (2010).

[57] A. Behranginia, Z. Hemmat, A. K. Majee, C. J. Foss, P. Yasaei, Z. Aksamija, and A. Salehi-Khojin, Power dissipation of WSe_2 field-effect transistors probed by low-frequency Raman thermometry, ACS Appl. Mater. Interfaces **10**, 24892 (2018).

[58] M.-L. Chen, X. Sun, H. Liu, H. Wang, Q. Zhu, S. Wang, H. Du, B. Dong, J. Zhang, Y. Sun, *et al.*, A FinFET with one atomic layer channel, Nat. Commun. **11**, 1205 (2020).

[59] L. Wang, A. R. Brown, M. Nedjalkov, C. Alexander, B. Cheng, C. Millar, and A. Asenov, in *2014 International Conference on Simulation of Semiconductor Processes and Devices (SISPAD)* (IEEE, Yokohama, Japan, 2014), p. 269.

[60] R. Rhyner and M. Luisier, Minimizing self-heating and heat dissipation in ultrascaled nanowire transistors, Nano Lett. **16**, 1022 (2016).

[61] Y. Sheng, Y. Hu, Z. Fan, and H. Bao, Size effect and transient phonon transport mechanism in approach-to-equilibrium molecular dynamics simulations, Phys. Rev. B **105**, 075301 (2022).

[62] N. K. Ravichandran, H. Zhang, and A. J. Minnich, Spectrally Resolved Specular Reflections of Thermal Phonons from Atomically Rough Surfaces, Phys. Rev. X **8**, 041004 (2018).

[63] C. Shao, Q. Rong, N. Li, and H. Bao, Understanding the mechanism of diffuse phonon scattering at disordered surfaces by atomistic wave-packet investigation, Phys. Rev. B **98**, 155418 (2018).

[64] H. Xie, M. Hu, and H. Bao, Thermal conductivity of silicene from first-principles, Appl. Phys. Lett. **104**, 131906 (2014).

[65] S. Li, Z. Tong, and H. Bao, Resolving different scattering effects on the thermal and electrical transport in doped SnSe, J. Appl. Phys. **126**, 025111 (2019).

[66] W. Li, J. Carrete, N. A. Katcho, and N. Mingo, ShengBTE: A solver of the Boltzmann transport equation for phonons, Comput. Phys. Commun. **185**, 1747 (2014).

[67] Z. Tong, S. Li, X. Ruan, and H. Bao, Comprehensive first-principles analysis of phonon thermal conductivity and electron-phonon coupling in different metals, Phys. Rev B **100**, 144306 (2019).